Human Pathology (2019) **83**, 115–123

ELSEVIER

Human PATHOLOGY

www.elsevier.com/locate/humpath

Original contribution

Immune environment in serrated lesions of the colon: intraepithelial lymphocyte density, PD-1, and PD-L1 expression correlate with serrated neoplasia pathway progression☆,☆☆

Gabriel Acosta-Gonzalez MD[a], Madhu Ouseph MD, PhD[a], Kara Lombardo BS[a], Shaolei Lu MD[a], Jonathan Glickman MD, PhD[b], Murray B. Resnick MD, PhD[a,*]

[a]*Department of Pathology, Brown University Warren Alpert Medical School, Rhode Island Hospital, Providence, RI 02903, USA*
[b]*Harvard Medical School, Beth Israel Deaconess Medical Center, Boston, MA 02215, USA*

Received 6 June 2018; revised 17 August 2018; accepted 23 August 2018

Keywords:
Serrated neoplasia;
Colon;
Intraepithelial lymphocytes;
Programmed death ligand 1 (PD-L1);
Microsatellite instability (MSI)

Summary The serrated neoplasia pathway accounts for approximately 20% of colorectal carcinomas (CRCs). Sessile serrated adenomas (SSAs), the main precursor lesion of the serrated pathway, are molecularly driven by *MLH1* promoter methylation and microsatellite instability (MSI) in their progression to CRC. MSI-high (MSI-H) lesions are highly immunogenic and associated with a high density of tumor-infiltrating lymphocytes. Our study's aim was to determine how the kinetics of this immune environment relates to SSAs in their progression through low-grade (SSA-LD) to high-grade dysplasia (SSA-HD) and CRC. We analyzed 74 cases (16 CRCs, 14 SSAs-HD, and 44 SSAs-LD). Cases of hyperplastic polyp and SSA without dysplasia were analyzed for comparison. MSI status, intraepithelial lymphocyte (IEL) density, and immune checkpoint expression were assessed by immunohistochemistry for mismatch repair proteins, CD3, and PD-1/PD-L1, respectively. Average IEL density was 12, 18.6, 21.6, and 31 for SSA, SSA-LD, SSA-HD, and CRC, respectively, as opposed to 8.1 in normal colon ($P < .0001$). Average PD-1/PD-L1 lymphocytic expression was 1.1/1.0, 1.2/2.9, 4.8/6.9, and 12.4/15.2 in SSA, SSA-LD, SSA-HD, and CRC, respectively, compared with 0.5/0 in normal crypts ($P < .0001$). IEL and PD-1/PD-L1 lymphocytic expression values of MSI-H lesions were 22.6, 27.7, and 36.8, and 3/6.5, 6.2/10.6, and 18.3/17.6 in MSI-H SSA-LD, SSA-HD, and CRCs, respectively (P ranged from .0478 to .3529). PD-L1 epithelial expression was positive in 40% of SSAs, 59.1% of SSAs-LD, 100% of SSAs-HD, and 60% of CRCs ($P < .0001$). Increased IELs and PD-1/PD-L1 expression correlate with sequential progression of SSAs, through development of cytologic dysplasia, to CRC and MSI-H status.

☆ Competing interest: The authors do not have a proprietary interest and declare no conflict of interest related to this work.
☆☆ Funding/Support: Research reported in this publication was supported by the Molecular Pathology Core of the COBRE Center for Cancer Research Development funded by the National Institute of General Medical Sciences of the National Institutes of Health under Award Number P20GM103421.
* Corresponding author at: Department of Pathology, Rhode Island Hospital, 593 Eddy St, APC Bldg 12-111, Providence, RI 02903.
E-mail address: mresnick@lifespan.org (M. Resnick).

https://doi.org/10.1016/j.humpath.2018.08.020
0046-8177/

1. Introduction

The realization that serrated lesions progress from sessile serrated adenoma (SSA) to SSA with cytologic dysplasia (SSA-D) to invasive carcinoma led to recognition of the serrated pathway of colorectal carcinogenesis. SSAs, through stepwise progression through the aforementioned dysplasia-carcinoma sequence, give rise to most sporadic microsatellite unstable (MSI-H) colorectal adenocarcinomas (CRCs). Serrated pathway carcinomas can harbor diverse molecular alterations but commonly share *BRAF* mutation and a CpG island methylator phenotype that can result in either microsatellite unstable or microsatellite stable (MSS) CRCs as reviewed by Jass [1] and Snover [2]. *BRAF* activating mutation is an early event in the formation of an SSA from normal mucosa or possibly a microvesicular hyperplastic polyp (HP) precursor. Serrated neoplasia pathway progression from SSA to sporadic MSI-H CRC is subsequently driven by CpG island methylation of the *MLH1* promoter region, which results in epigenetic silencing and onset of DNA mismatch repair (MMR) deficiency. Once microsatellite instability (MSI) develops, lesions can rapidly accumulate additional mutations, coinciding with the development of dysplasia and progression to invasive carcinoma [1,2].

Microsatellite unstable carcinomas and carcinomas arising from the serrated pathway are frequently characterized by high numbers of tumor-infiltrating lymphocytes [3-5] and express the immune checkpoint receptor programmed death ligand 1 (PD-L1) [6,7]. However, few studies have examined the immune environment in both serrated and nonserrated precursor lesions [8,9]. Rau et al [8] were the first to study the immune environment in serrated precursor lesions, with an emphasis on tumor-infiltrating lymphocytes (TILs), whereas Rubio et al [9] analyzed TIL density in colorectal conventional adenomas with low- and high-grade dysplasia, and carcinomas. However, no studies have analyzed immune checkpoint protein expression, particularly PD-1/PD-L1, in precursor serrated lesions and its relationship to the onset of MSI-H status and morphologic dysplasia. Therefore, the objective of this study was to examine the density of intraepithelial lymphocytes (IELs), expression of PD-1 in infiltrating lymphocytes, expression of PD-L1 in infiltrating lymphocytes and lesion epithelium, and MSI status at various stages of progression through the serrated neoplasia pathway.

2. Materials and methods

2.1. Patients and samples

Study cases were identified by retrospective search of pathology databases at Rhode Island Hospital and Miriam Hospital over a 10-year period and at Beth Israel Deaconess Medical Center over 3 years using keywords "sessile serrated adenoma" or "sessile serrated polyp" in combination with "dysplasia" or "carcinoma." A total of 74 cases, including both biopsy and resection specimens, of SSAs associated with cytologic dysplasia or invasive carcinoma were analyzed. This included 44 SSAs with low-grade dysplasia (SSAs-LD), 14 SSAs with high-grade dysplasia (SSAs-HD), and 16 adenocarcinomas (ACAs). Ten cases each of HP and SSA without dysplasia were prospectively identified during routine pathologic evaluation and included for comparison. Pathology and endoscopy reports were reviewed for patient clinical features, including age at diagnosis, sex, and anatomic location. No cases of Lynch syndrome were included. Left-sided neoplasia was defined as polyps or cancer arising from the splenic flexure distally, and right sided neoplasia was defined as those proximal to the splenic flexure.

This study was performed under a protocol approved by the institutional review boards of Rhode Island Hospital and Beth Israel Deaconess Medical Center.

2.2. Histomorphologic subtypes

Hematoxylin and eosin–stained slides of potential study cases were retrieved and reviewed by 2 independent gastrointestinal pathologists for subtype classification through strict assessment of cytological and architectural features. Criteria for SSAs-LD and SSAs-HD study inclusion included presence of areas with serrated architecture, characterized by luminal in-folding or "saw-tooth" appearance of epithelium, and at least 1 unequivocal architecturally distorted crypt with basal dilatation and/or horizontal branching (particularly if associated with inverted maturation or asymmetric proliferation zone) [10]. In addition, a transition to cytologically dysplastic areas within the same tissue fragment displaying architectural features described above was a requisite for study inclusion. Representative examples of histomorphologic classification subtypes are shown in Fig. 1. Cases with separate tissue fragments with dysplasia and serrated architecture, but no single fragment displaying both, were excluded. ACAs with associated architecturally unequivocal areas of SSA with contiguous or abrupt transition to cytologic dysplasia in the vicinity of invasion met the study criteria and were included as serrated neoplasia pathway ACAs.

2.3. Immunohistochemistry

Table 1 contains a summary of the immunohistochemical stains used. In brief, stains for each antigen were performed on 4-μm paraffin tissue sections. The panel included antibodies against CD3, PD-1, PD-L1, PMS2, and MSH6. The stains were loaded on the Ventana XT Autostainer (Roche, Switzerland) and run to completion using the Discovery DabMap Detection Kit (Roche).

2.3.1. Immunohistochemical assessment and scoring

IEL density, corresponding to highest-density area of CD3-positive cells, and intraepithelial lymphocytic expression of

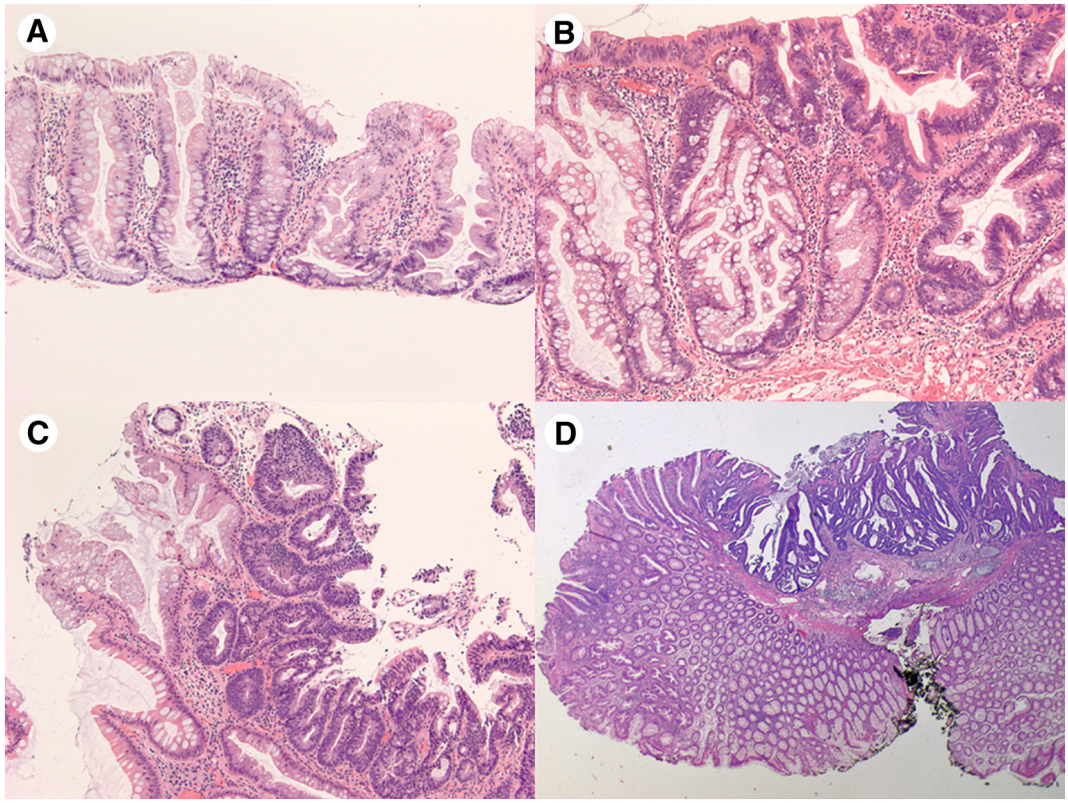

Fig. 1 Serrated neoplasia morphologic dysplasia to carcinoma stepwise progression. A, SSA (hematoxylin and eosin [H&E], original magnification ×100). B, SSA-LD (H&E, ×100). C, SSA-HD (H&E, ×100). D, ACA arising from SSA (H&E, ×20).

PD-1 and PD-L1 per 200 epithelial cells were separately scored for areas of HP, SSA, SSA-LD, SSA-HD, and ACA, and also for areas corresponding to MSI-H. Normal adjacent colonic crypts were also scored for internal control purposes. Extent and intensity of PD-L1 expression in epithelium were scored semiquantitatively in the different morphologic areas. The extent of epithelial PD-L1 membranous staining, either complete or apical, was semiquantitatively scored from 0 to 3 according to the percentage of staining cells (0, 0%; 1, <25%; 2, 25%-50%; 3, >50%). Epithelial PD-L1 staining intensity was considered weak if there was absent or barely perceptible staining at ×10 magnification, moderate if easily identifiable at ×10 magnification, and intense if easily identifiable at ×4 magnification. Only cases with moderate-to-intense staining intensity were considered positive. A 2-panel test for PMS2 and MSH6 expression by immunohistochemistry (IHC) was used to evaluate MSI status in serrated precursor lesions. The sensitivity and specificity of the 2 panel test as a screen for MSI approached 100% when compared with the traditional 4-panel test [11]. Carcinomas were tested for all 4 MMR proteins (MLH1, PMS2, MSH2, and MSH6) by IHC to assess MSI status.

Table 1 Summary of antibodies and methods

Antibody	Source	Host	Antigen retrieval	Dilution	Detection method
CD3	Dako, Carpinteria, CA	Rabbit polyclonal	EDTA pH 9 100°C, 40 min	RTU	Ventana XT DabMap Kit
PD1	Abcam, Cambridge, MA	Mouse monoclonal, clone NAT105	EDTA pH 9 100°C, 40 min	1:100	Ventana XT DabMap Kit
PDL1	Abcam	Rabbit monoclonal, clone EPR1161	EDTA pH 9 100°C, 40 min	1:1500	Ventana XT DabMap Kit
MSH6	Dako	Rabbit monoclonal, clone EP49	EDTA pH 9 100°C, 40 min	RTU	Ventana XT DabMap Kit
PMS2	Dako	Rabbit monoclonal, clone EP51	EDTA pH 9 100°C, 40 min	RTU	Ventana XT DabMap Kit

2.4. Statistical analysis

Statistical analysis included mean values for CD3 IEL density, PD-1 and PD-L1 lymphocytic expression, and percentage positive cases for PD-L1 epithelial expression, which were measured within each histopathologic lesion subtype and according to MSI status. Results were compared using analysis of variance (ANOVA; followed by Tukey pairwise comparison if necessary), *t* test, and χ^2 test (followed by Fisher exact test if necessary). All statistical analyses were done using JMP Pro 13.0 (Cary, NC). $P < .05$ was considered statistically significant.

3. Results

3.1. Clinicopathological features

The clinicopathological features are summarized in Table 2. The mean patient age increased with lesion progression, with means of 58 years for HPs, 57 years for SSAs, 65 years for SSAs-LD, 72 years for SSAs-HD, and 77 yr. for ACAs with serrated precursor lesions ($P < .0001$). Sixty-five (69%) of the 94 included cases were from female patients, including 40% of HPs, 80% of SSAs, 66% of SSAs-LD, 71% of SSAs-HD, and 88% of ACAs. Excluding HPs, which were all located in the sigmoid or rectum, most lesions were located in the right colon (81%).

3.2. Immunohistochemistry

3.2.1. Correlation of IEL density with serrated neoplasia pathway progression

CD3-positive IEL density correlated with progression of serrated pathway precursor lesions, HPs to SSAs, through the dysplasia-carcinoma sequence (Fig. 2, Table 2). Mean IEL density was 12.9 per 200 epithelial cells in HPs and 12 in SSAs compared with 8.1 in normal adjacent colonic crypts. The IEL density increased to 18.6 in SSAs-LD, 21.6 in SSAs-HD, and 31 in CRCs, showing a statistically significant trend ($P < .0001$). An example of CD3-positive intraepithelial lymphocytic distribution is seen in Supplementary Fig. 1.

Table 2 Clinical characteristics and marker expression of study lesions

	Normal (n = 78)	HP (n = 10)	SSA-ND (n = 10)	SSA-LD (n = 44)	SSA-HD (n = 14)	ACA (n = 16)	*P*
Age (y)							<.0001
Mean	NA	58	57	65	72	77	
SEM		3.0	3.0	1.5	3.3	2.0	
Sex							.1150
Female	NA	4 (40%)	8 (80%)	29 (65.9%)	10 (71.4%)	14 (87.5%)	
Male		6 (60%)	2 (20%)	15 (34.1%)	4 (28.6%)	2 (12.5%)	
Location							<.0001
Right	NA	0	7 (70%)	33 (75%)	13 (92.8%)	14 (87.5%)	
Left		10 (100%)	3 (30%)	11 (25%)	1 (7.2%)	2 (12.5%)	
IEL (CD3+)							<.0001
Mean	8.1	12.9	12	18.6	21.6	31 [a]	
SEM	0.6	1.5	1.8	1.4	3.5	5.3	
PD-1							<.0001 [b]
Mean	0.5	0	1.1	1.2	4.8	12.4	
SEM	0.1	0	0.4	0.4	1.8	4.3	
PD-L1							<.0001 [c]
Mean	0	0.2	1	2.92	6.91	15.26	
SEM	0	0.13	0.33	0.55	1.78	2.09	
PD-L1(E)							.0008 [d]
Negative	28 (73.7%)	5 (50%)	6 (60%)	9 (40.9%)	0	6 (40%)	
Positive	10 (26.3%)	5 (50%)	4 (40%)	13 (59.1%)	9 (100%)	9 (60%)	
MSI status							.0001 [d]
MSS	NA	NA	NA	38 (88.4%)	7 (50%)	6 (37.5%)	
MSI-H				5 (11.6%)	7 (50%)	10 (62.5%)	

Abbreviation: NA, not applicable.

[a] ANOVA followed by Tukey pairwise comparison: the ACA group had significantly more IELs than did the normal crypt, HP, SSA-ND, and SSA-LD groups. The normal crypt group had significantly less IEL than did the SSA-LD, SSA-HD, and ACA groups.

[b] ANOVA followed by Tukey pairwise comparison: the ACA group had significantly more PD-1(+) IELs than did all the other groups.

[c] ANOVA followed by Tukey pairwise comparison: the ACA group had significantly more PD-L1(+) IELs than did all the other groups; the SSA-HD group had significantly more PD-L1(+) IELs than did the SSA, HP, and NL groups; the SSA-LD group had significantly more PD-L1(+) IELs than did the SSA, HP, and NL groups.

[d] Fisher exact test.

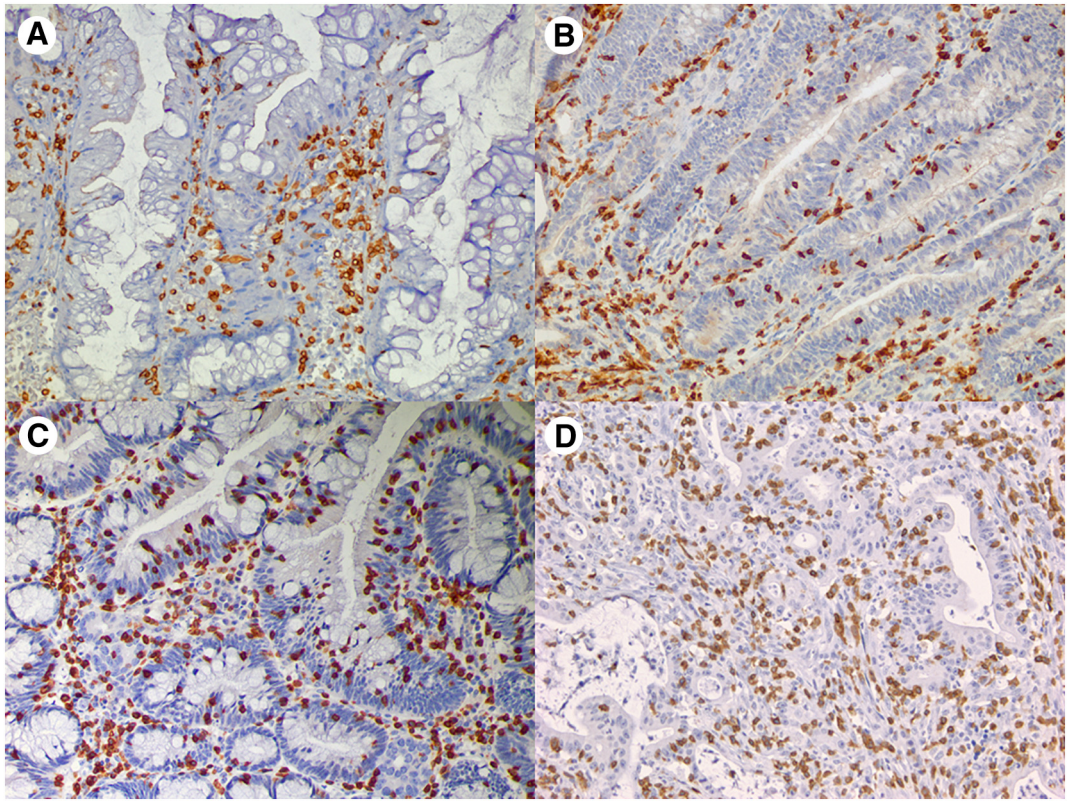

Fig. 2 IEL density in serrated neoplasia pathway progression. A, SSA (CD3 IHC, original magnification ×200). B, SSA-LD (CD3 IHC, ×200). C, SSA-HD (CD3 IHC, ×200). D, ACA arising from SSA (CD3 IHC, ×200).

3.2.2. Correlation of PD-1 and PD-L1 lymphocytic expression with serrated neoplasia pathway progression

PD-1 and PD-L1 expressions within IELs, corresponding to highest IEL density area by CD3 immunostain, were also scored separately for all different histomorphologic lesion subtypes. Similar to IEL density results, PD-1 and PD-L1 expressions within lymphocytes increased with stepwise progression through serrated carcinogenesis (Figs. 3 and 4, Table 2). Although none of the 10 cases of HPs assessed showed PD-1 expression, mean values increased from 1.1 to 1.2, 4.8, and 12.4 in SSA, SSA-LD, SSA-HD, and CRC, respectively, compared with mean PD-1 lymphocytic expression of 0.5 in normal colonic epithelium ($P < .0001$). The extent of PD-L1 expression within lymphocytes showed a similar trend within serrated pathway lesions, with values of 1.0, 2.9, 6.9, and 15.3 in SSAs, SSAs-LD, SSAs-HD, and CRC, respectively, compared with 0 in normal colonic mucosa ($P < .0001$).

3.2.3. Correlation of PD-L1 epithelial expression with serrated neoplasia pathway progression

Lesions were scored as positive for PD-L1 expression in epithelium (at least moderate staining in 25% of cells) in 50% of HPs, 40% of SSAs, 59.1% of SSAs-LD, 100% of SSAs-HD, and 60% of ACAs compared with 26.3% in nonlesional colonic epithelium ($P = .008$; refer to Fig. 5 and Table 2). PD-L1 epithelial positivity showed an overall upward trend with increased lesion severity.

3.3. Correlation of MSI with immune microenvironment

Results of MSI status correlation with immune microenvironment are summarized in Table 3. A total of 22 (29.7%) of the 74 study cases showed immunohistochemical evidence of MSI, with all cases showing loss of expression of MMR protein PMS2. Among the 22 total MSI-H cases, there were 5 SSAs-LD (11%), 7 SSAs-HD (50%), and 10 CRCs (62%). The onset of MSI had the strongest association with increased IEL density and lymphocytic PD-1/PD-L1 expression. Mean IEL densities were 22.6, 27.7, and 36.8 for MSI-H SSAs-LD, SSAs-HD, and CRCs, respectively. In comparison, MSS counterparts mean IEL values were 18, 15.6, and 21.3 ($P = .546$). Similarly, PD-1/PD-L1 lymphocytic expression values were 3/6.5, 6.2/10.6, and 18.3/17.6 ($P = .2964$ and $P = .0478$, respectively) for MSI-H SSAs-LD, SSAs-HD, and CRCs, respectively. Corresponding results for MSS lesions were 1.1/2.3, 3/1.8, and 4.7/11.8 ($P = .022$ and $P < .0001$, respectively). Epithelial PD-L1 expression was also higher in MSI-H lesions, with 21 (95%) of the 22 MSI-H cases positive for PD-L1 expression compared with 44 (85%) of 52 MSS SSAs-D/CRC cases. Of note, individual study cases with areas of intact MMR protein expression adjacent to areas with lost expression showed this same pattern, with higher IEL density and PD-1/PD-L1 expression corresponding to MSI-H areas when compared with MSS regions within the same slide (Fig. 5).

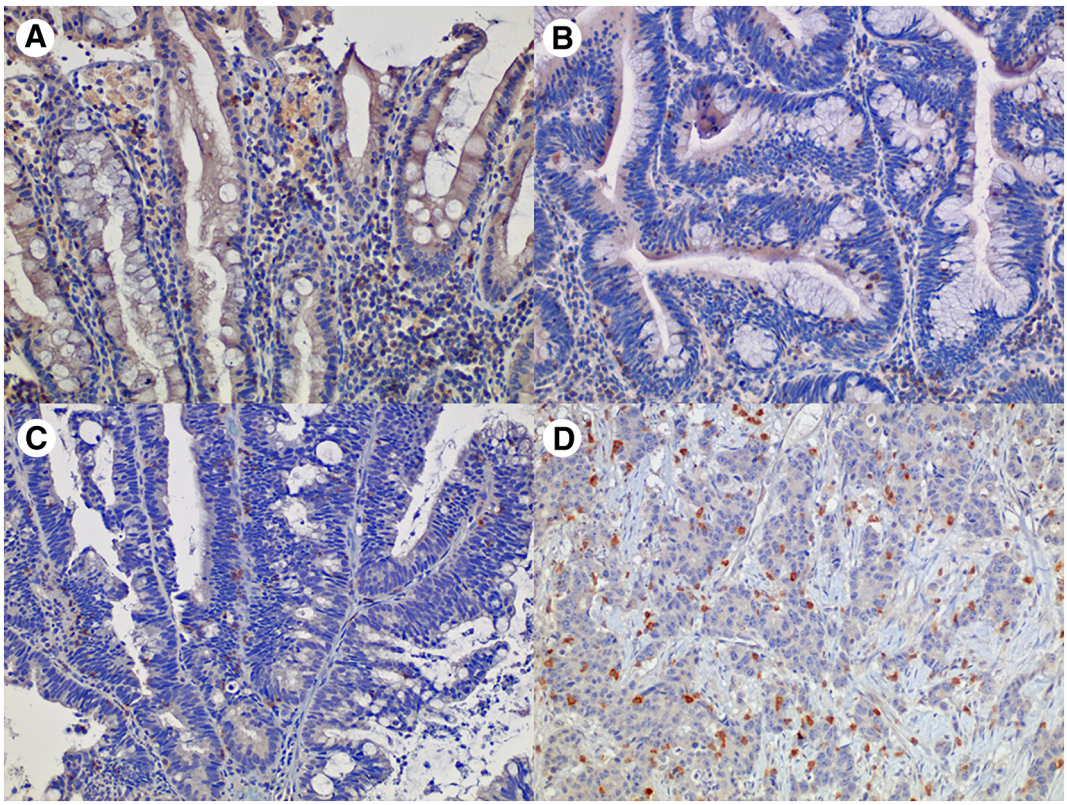

Fig. 3 Intraepithelial PD-1 lymphocytic expression in serrated neoplasia pathway progression. A, SSA (PD-1 IHC, original magnification ×200). B, SSA-LD (PD-1 IHC, ×200). C, SSA-HD (PD-1 IHC, ×200). D, ACA arising from SSA (PD-1 IHC, ×200).

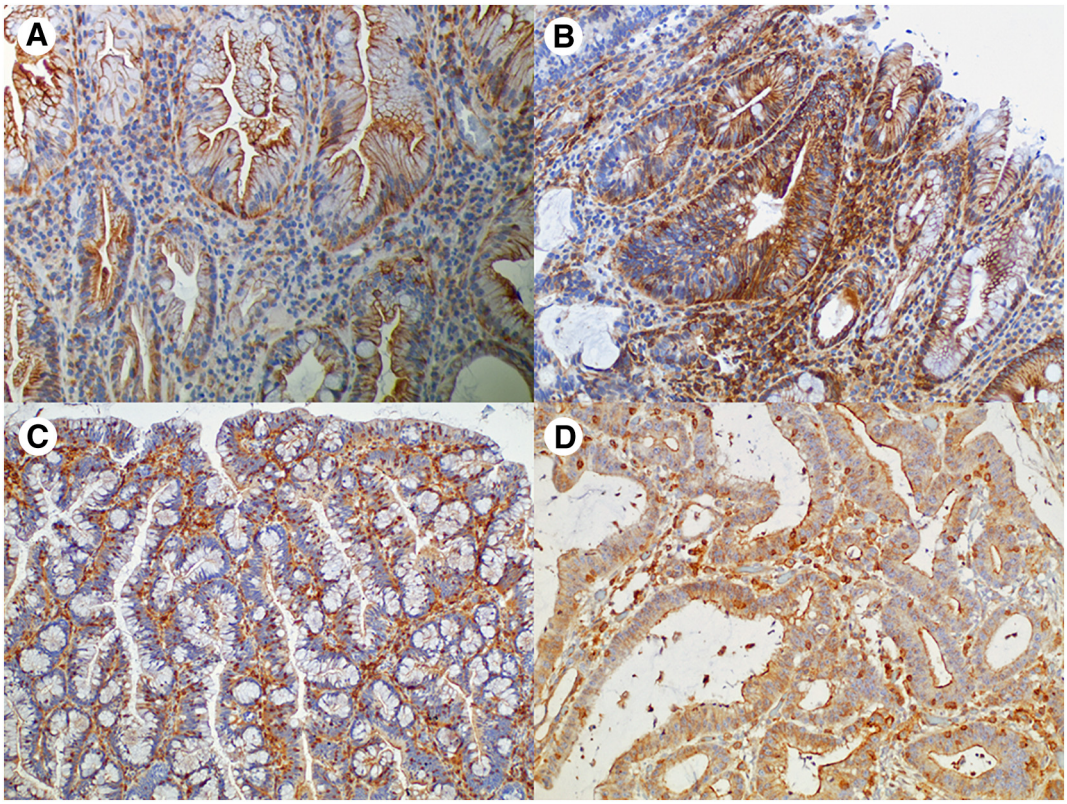

Fig. 4 Epithelial and intraepithelial PD-L1 lymphocytic expression in serrated neoplasia pathway progression. A, SSA (PD-L1 IHC, original magnification ×200). B, SSA-LD (PD-L1 IHC, ×200). C, SSA-HD (PD-L1 IHC, ×200). D, ACA arising from SSA (PD-L1 IHC, ×200).

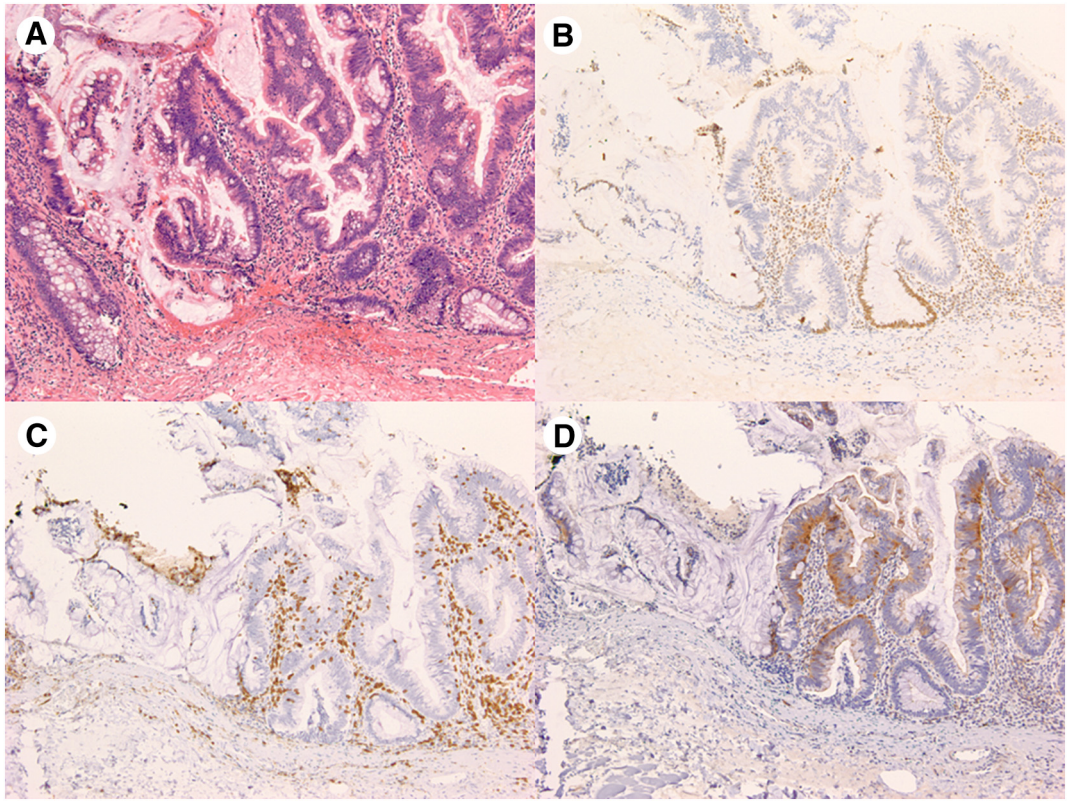

Fig. 5 Immune microenvironment of serrated neoplasia pathway with onset of MSI. A, SSA with abrupt transition to low-grade dysplasia (hematoxylin and eosin, original magnification ×100). B, SSA-LD showing loss of PMS2 expression in dysplasia component (PMS2 IHC, ×100). C, Higher IEL density in area of SSA-LD with MSI versus adjacent area of SSA with intact MMR protein expression (CD3 IHC, ×100). D, Increased PD-L1 epithelial and lymphocytic PD-L1 expression in area of SSA-LD with MSI versus adjacent area of SSA with intact MMR protein expression (PD-L1 IHC, ×100).

4. Discussion

In our study, we set out to evaluate immune features of the serrated carcinogenesis pathway and their correlation with morphologic stepwise dysplasia-carcinoma progression and MSI status. To our knowledge, this is the first study to look at immune checkpoint expression patterns in serrated precursor lesions, by analyzing expression patterns of PD-1 and PD-L1 in serrated carcinogenesis and how these relate to lesion progression, dysplasia, and MSI-H status. Of note, although onset of MSI is classically associated with progression to carcinoma, a significant proportion of carcinomas that arise through the serrated pathway are MSS, which we also include in our study. Very few studies have analyzed the particulars of the immune microenvironment of these MSS serrated carcinomas.

Our results show that IEL density, lymphocytic PD-1/PD-L1, and epithelial PD-L1 expression increase as lesions sequentially progress through the dysplasia-carcinoma sequence of serrated carcinogenesis. Our findings of increased IEL density with serrated neoplasia progression are in line with those previously described by Rau et al [8]. We also demonstrate a strong correlation of increased IEL density and immune checkpoint expression with MSI-H status, as MSI-H SSAs-D and CRCs had significantly higher IEL density values and PD-1/PD-L1 expression when compared with MSS serrated carcinomas. Interestingly, we found that increased numbers of IELs, including PD-1 and PD-L1 expressing IELs, and PD-L1 epithelial expression can be seen before the

Table 3 IEL populations in colonic neoplasm based on MSI status

Markers	SSA-LD (44)	SSA-HD (14)	ACA (16)	*P*
PD-L1(+) IEL				
MSS	2.3 ± 0.5	1.8 ± 0.6	11.8 ± 1.9	<.0001 [a]
MSI-H	6.5 ± 2.0	10.6 ± 2.1	17.6 ± 3.1	.0478 [b]
PD-1(+) IEL				
MSS	1.1 ± 0.5	3.0 ± 2.1	4.7 ± 1.5	.022 [c]
MSI-H	3.0 ± 0	6.2 ± 2.7	18.3 ± 8.0	.2964
CD3(+) IEL				
MSS	18.0 ± 1.4	15.6 ± 1.7	21.3 ± 7.3	.546
MSI-H	22.6 ± 6.2	27.7 ± 6.2	36.8 ± 6.8	.3529

[a] Tukey pairwise comparison: the ACA group had significantly more PD-L1(+) IELs than did the SSA-LD and SSA-HD groups. No difference was seen between the SSA-LD group and the SSA-HD group.

[b] Tukey pairwise comparison: no significant difference between individual groups.

[c] Tukey pairwise comparison: the ACA group had significantly more PD-1(+) IELs than did the SSA-LD group.

development of MMR loss. Thus, infiltration of lymphocytes and upregulation of PD-L1 in precursor lesions is not solely dependent on generation of immunogenic neoantigens resulting from MMR deficiency, but is likely dependent on earlier, as yet undefined, molecular mechanisms.

The serrated neoplasia pathway is 1 of 2 major morphologic stepwise colorectal carcinogenesis pathways, accounting for approximately 20% of all CRCs. Presently, SSAs are recognized as premalignant lesions associated with distinct molecular alterations in their progression to CRC. SSAs commonly harbor somatic *BRAF* mutations and arise within a background of global genome hypermethylation as reviewed by Jass [1] and Snover [2]. Molecularly, this epigenetic instability is the main driver of serrated neoplasia pathway progression. By means of a yet unknown initiating mutation or epigenetic event, vast promoter CpG island hypermethylation leads to progressive silencing of tumor suppressor genes and a CpG island methylator phenotype [12]. When and if hypermethylation of the *MLH1* gene promoter occurs, gene expression is silenced and MMR deficiency ensues. The onset of MMR deficiency and subsequently MSI serves as a major boost in serrated lesion carcinogenesis. The hypermutator phenotype characteristic of MSI-H lesions results in mutation burden accumulation, increasing the probability of progression to carcinoma [13]. Morphologically, this progression manifests in SSAs by development of cytologic adenomatous dysplasia, with stepwise progression from SSA-LD to SSA-HD, and ultimately carcinoma (ACA) [14,15].

SSAs-D are the intermediate lesion in the progression of SSAs to CRC through serrated carcinogenesis. SSAs-D are molecularly advanced lesions that frequently harbor MSI with loss of MLH1 expression and are associated with significantly higher rates of invasive carcinoma than conventional adenomas [16]. A recent study evaluated MLH1 expression by IHC in SSAs-D and found that 73% of 266 analyzed lesions had loss of MLH1, whereas 19% were associated with invasive carcinoma [17]. In addition, other studies have shown retained expression of MLH1 in areas of SSA with concomitant loss within areas of dysplasia within the same lesion, suggesting that onset of MSI is an important driver in the dysplasia-carcinoma progression [18,19].

Onset of MMR deficiency and MSI-H phenotype leads to accumulation of frameshift mutations within microsatellites located in coding regions of tumor cell DNA. As neoplastic cells proliferate and divide, previously unrecognized new "nonself" or neoantigens are produced, setting off a powerful immune response and acting as a homing factor that attract numerous TILs that have been primed for an antitumor cytotoxic response. Indeed, studies of the immune environment in CRCs with MSI have shown that MSI-H tumors are associated with a higher density of TILs than MSS lesions [3-5] and that these TILs are often cytotoxic and activated [20,21]. In addition, other studies have shown that overall number of frameshift mutations in CRCs with MSI correlates with tumor-infiltrating lymphocyte density, specifically CD8+ lymphocyte density [22,23].

Although the MSI tumor microenvironment is rich in antitumor TILs, multiple anti-immune counterregulatory pathways (PD-1/PD-L1, IDO-1) may limit immune response and resist tumor elimination. Up-regulation of immune checkpoints, which are a constellation of different intrinsic immune inhibitory pathways designed to maintain self-tolerance and prevent damage to our own healthy tissues [24], by tumor cells counter the initial host cytotoxic response and allow neoplastic cells to evade the immune system. Llosa et al [25] showed that the immune environment in MSI CRCs is highly active and that tumors can escape the immune response through up-regulated expression of multiple different immune checkpoint ligands. This was further supported by a study of medullary CRC that showed increased expression of immune checkpoint ligands IDO and PD-L1 in medullary tumor cells and greater numbers of CD8+, PD-1+, PD-L1+, and FoxP3+ TILs, highlighting the complexity and dynamism of the immune microenvironment of MSI CRCs [26].

The PD-1/PD-L1 and programmed death ligand-2 (PD-L2) is one of the most important and currently studied checkpoints. In the PD-1 pathway, interaction between the PD-1 receptor expressed on the surface of T cells, and PD-L1/PD-L2 ligands expressed on the tumor cell surface renders T cells inactive. Studies have shown that MMR-deficient tumors have significantly higher rates of PD-L1 and lymphocytic PD-1 expression when compared with MMR-proficient tumors [6]. PD-L1 expression in CRC is also associated with clinicopathological and molecular features of the serrated pathway of colorectal carcinogenesis. Specifically, PD-L1 expression in CRCs is associated with high TIL density, BRAF mutation, medullary morphology, and MSI [7].

Although many studies have analyzed the immune landscape of CRCs with MSI, only one study evaluated the immune microenvironment of serrated precursor lesions, including SSAs with dysplasia (SSAs-D) [8]. Rau et al [8] examined IEL density in different serrated polyps and SSAs-D. The authors found that numbers of IELs were significantly higher in SSA-D compared with SSAs, which in turn showed significantly greater numbers of IELs when compared with HPs and conventional adenomas.

In conclusion, our results show that increased IEL density and PD-1/PD-L1 expression correlate with progression of SSAs to SSAs-D to CRC, and particularly with MSI-H status. Our findings support the stepwise dysplasia-carcinoma sequence of serrated carcinogenesis and the hypermutator phenotype mechanism of MSI-H lesions, which stimulates a host immune response characterized by brisk lymphocytic infiltration counterbalanced by immune checkpoint expression up-regulation by neoplastic cells.

Supplementary data

Supplementary data to this article can be found online at https://doi.org/10.1016/j.humpath.2018.08.020.

References

[1] Jass JR. Classification of colorectal cancer based on correlation of clinical, morphological and molecular features. Histopathology 2007;50:113-30.

[2] Snover DC. Update on the serrated pathway to colorectal carcinoma. Hum Pathol 2011;42:1-10.

[3] Greenson JK, Bonner JD, Ben-Yzhak O, et al. Phenotype of microsatellite unstable colorectal carcinomas: well-differentiated and focally mucinous tumors and the absence of dirty necrosis correlate with microsatellite instability. Am J Surg Pathol 2003;27:563-70.

[4] Greenson JK, Huang SC, Herron C, et al. Pathologic predictors of microsatellite instability in colorectal cancer. Am J Surg Pathol 2009;33:126-33.

[5] Shia J, Ellis NA, Paty PB, et al. Value of histopathology in predicting microsatellite instability in hereditary nonpolyposis colorectal cancer and sporadic colorectal cancer. Am J Surg Pathol 2003;27:1407-17.

[6] Lee LH, Cavalcanti MS, Segal NH, et al. Patterns and prognostic relevance of PD-1 and PD-L1 expression in colorectal carcinoma. Mod Pathol 2016;29:1433-42.

[7] Rosenbaum MW, Bledsoe JR, Morales-Oyarvide V, Huynh TG, Mino-Kenudson M. PD-L1 expression in colorectal cancer is associated with microsatellite instability, BRAF mutation, medullary morphology and cytotoxic tumor-infiltrating lymphocytes. Mod Pathol 2016;29:1104-12.

[8] Rau TT, Atreya R, Aust D, et al. Inflammatory response in serrated precursor lesions of the colon classified according to WHO entities, clinical parameters and phenotype-genotype correlation. J Pathol Clin Res 2016;2:113-24.

[9] Rubio CA, Jacobsson B, Castanos-Velez E. Cytotoxic intraepithelial lymphocytes in colorectal polyps and carcinomas. Anticancer Res 1999;19:3221-7.

[10] Rex DK, Ahnen DJ, Baron JA, et al. Serrated lesions of the colorectum: review and recommendations from an expert panel. Am J Gastroenterol 2012;107:1315-29.

[11] Hall G, Clarkson A, Shi A, et al. Immunohistochemistry for PMS2 and MSH6 alone can replace a four antibody panel for mismatch repair deficiency screening in colorectal adenocarcinoma. Pathology 2010;42:409-13.

[12] Hawkins N, Norrie M, Cheong K, et al. CpG island methylation in sporadic colorectal cancer and its relationship to microsatellite instability. Gastroenterology 2002;122:1376-87.

[13] Maeda T, Suzuki K, Togashi K, et al. Sessile serrated adenoma shares similar genetic and epigenetic features with microsatellite unstable colon cancer in a location-dependent manner. Exp Ther Med 2011;2:695-700.

[14] Jass JR, Baker K, Zlobec I, et al. Advanced colorectal polyps with the molecular and morphological features of serrated polyps and adenomas: concept of a 'fusion' pathway to colorectal cancer. Histopathology 2006;49:121-31.

[15] Goldstein NS. Small colonic microsatellite unstable adenocarcinomas and high-grade epithelial dysplasias in sessile serrated adenoma polypectomy specimens: a study of eight cases. Am J Clin Pathol 2006;125:132-45.

[16] Cenaj O, Gibson J, Odze RD. Clinicopathologic and outcome study of sessile serrated adenomas/polyps with serrated versus intestinal dysplasia. Mod Pathol 2018;31:633-42.

[17] Liu C, Walker NI, Leggett BA, Whitehall VLJ, Bettington ML, Rosty C. Sessile serrated adenomas with dysplasia: morphological patterns and correlations with MLH1 immunohistochemistry. Mod Pathol 2017;30:1728-38.

[18] Sheridan TB, Fenton H, Lewin MR, et al. Sessile serrated adenomas with low- and high-grade dysplasia and early carcinomas: an immunohistochemical study of serrated lesions "caught in the act". Am J Clin Pathol 2006;126:564-71.

[19] Fujita K, Yamamoto H, Matsumoto T, et al. Sessile serrated adenoma with early neoplastic progression: a clinicopathologic and molecular study. Am J Surg Pathol 2011;35:295-304.

[20] Alexander J, Watanabe T, Wu TT, Rashid A, Li S, Hamilton SR. Histopathological identification of colon cancer with microsatellite instability. Am J Pathol 2001;158:527-35.

[21] Phillips SM, Banerjea A, Feakins R, Li SR, Bustin SA, Dorudi S. Tumour-infiltrating lymphocytes in colorectal cancer with microsatellite instability are activated and cytotoxic. Br J Surg 2004;91:469-75.

[22] Tougeron D, Fauquembergue E, Rouquette A, et al. Tumor-infiltrating lymphocytes in colorectal cancers with microsatellite instability are correlated with the number and spectrum of frameshift mutations. Mod Pathol 2009;22:1186-95.

[23] Maby P, Tougeron D, Hamieh M, et al. Correlation between density of CD8 T-cell infiltrate in microsatellite unstable colorectal cancers and frameshift mutations: a rationale for personalized immunotherapy. Cancer Res 2015;75:3446-55.

[24] Pardoll DM. The blockade of immune checkpoints in cancer immunotherapy. Nat Rev Cancer 2012;12:252-64.

[25] Llosa NJ, Cruise M, Tam A, et al. The vigorous immune microenvironment of microsatellite instable colon cancer is balanced by multiple counter-inhibitory checkpoints. Cancer Discov 2015;5:43-51.

[26] Friedman K, Brodsky AS, Lu S, et al. Medullary carcinoma of the colon: a distinct morphology reveals a distinctive immunoregulatory microenvironment. Mod Pathol 2016;29:528-41.